

# LONG -TERM LOADING CREEP TEST ON A FULL -SCALE STEEL BAR TIMBER COMPOSITE BEAM

Takeshi Izaki<sup>1</sup>, Shinichi Shioya<sup>2</sup>

**ABSTRACT:** We have been developing a frame system formed by timber members strengthened by deformed steel bars using epoxy resin adhesive. We have reported the creep test of small-scaled specimens of composite timber beams in WCTE2018 and WCTE2021. We have been conducting, from December 2023, a new creep test for one full-scale section- and large-span-composite beam specimen and one full-scale section Glulam timber beam specimen under a natural-variable environment by 4-point bending loading. They have been adjusted to same long-term allowable bending moment of wood at mid span of each beam and allowable shear force at both lefthand and righthand shear spans by selecting the lengths of beam and the shear spans. This paper reports approximately one-year results of the creep test of full-scale beam specimens and curvature-elapsed time curve, for the composite timber beam, calculated by using curvature-elapsed time curve of the glulam timber beam.

**KEYWORDS:** Composite timber Beam, Deformed steel bar, Bending creep, Full-scale

## 1 – INTRODUCTION

S. Shioya *et al.* have been developing a steel bar-timber composite member system which increases its bending stiffness and strength by gluing rebars to outer within cedar Glulam timber [1]. We expect that the rebar in the composite beam can not only increase its bending stiffness and strength but also decrease its bending creep. We carried out long-term loading tests with small-scale specimens (1/4 of scale) to clarify the reduction of creep deflection with the rebars and propose a method for estimating the deflection [2].

A first purpose of this study is to verify the validity of the estimation method with full-scale size beam specimens. In the test using small-scale specimens, a decrease of the shearing stiffness (adhesion stiffness) of a wood portion around rebar within the specimen during the rainy season, caused a decrease in the rebar resistance and an increase in deflection. The cause was the moisture absorption of the wood portion around rebar, and on the wood surface, so it was required to take measures to prevent the absorption. In Japan's rainy season, the depth of water seepage from the wood surface is approximately 16 mm. In actual composite timber beams with full size, the rebars are, in general, at depths than the 16mm depth from the surface of beam, so it is predicted that no measures to prevent the moisture absorption are probably required.

A second purpose is to investigate whether, in full-scale beams, the protection for the moisture absorption is required or not. We have been performing a long-term loading creep test with a full-scale composite beam since December in 2023 for the verification of them. This paper reports the experiment, its results, the relative creep coefficient of the composite beam, and its estimation. For previous research and other's research on the creep of composite wood beams such as hybrid timber beams, please refer to Reference [2].

## 2 – EXPERIMENT

### 2.1 AIM

Its shear deformation of the beam is significantly large compared with bending deformation against that of a conventional timber beam because the shear stress with which a composite timber beam is subjected to creep test loading is large. Accordingly, the estimation of the deflection of the composite beams is necessary to estimate separately bending and shear deformation components. The estimation of the creep deflection is also required to be separated into the components. It is important to estimate the bending deformation in the creep deflection because the rebars mainly decrease the bending deformation. Determining the relative creep coefficient of the composite beam should be based on the

---

<sup>1</sup> Takeshi Izaki 1, Department of Architecture, Kagoshima University, Kagoshima, Japan, izaki@eng.kagoshima-u.ac.jp

<sup>2</sup> Shinichi Shioya 2, Department of Architecture, Kagoshima University, Kagoshima, Japan, k7347039@kadai.jp

data of many of specimens from variations in wood properties. However, it requires large specimens and the apparatus for applying large load and performing the test with many full-scale specimens is very hard. Therefore, we devised a process to collect multiple data in an experiment using a single specimen. Glulam timber is manufactured by gluing dried and graded lumber cut from various trees of the same species. There are some variations of wood properties depending on even positions within a specimen as a matter of course. In the four-point flexural test with one beam, measure of axial strains of wood at a large number of locations within the pure bending span in the specimen give a number of moment-curvature relationships. The variation of data of moment-curvature relationship affects the variation of bending deflection of the beam. The rebars, also, make uniform the shear stress distribution, therefore reducing shear deformation in the beam. In the shear span of the beam, shear deformation components can be calculated in the same way as the bending deformation. The probability density distributions of the deflection and creep components of timber beams can be obtained from the average, maximum, minimum, and distribution of each component of a single beam, and the variation of these components can also be estimated. On this research, using curvature data at many positions obtained from a long-term loading test with one full-scale composite timber beam, we verify the validity of the previous proposed method for estimating bending creep deformation and investigate effect of moisture absorption of the wood portion around rebar to the creep above.

## 2.2 COMPONENT OF DEFLECTION DURING LONG TERM LOADING

The relative creep coefficient of curvature,  $C_\phi$ , is expressed by Equation (1), as proposed in the previous paper [2].

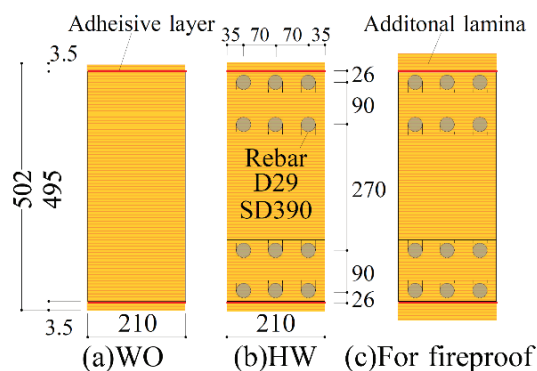
$$C_\phi = (1.0 + EI_s/EI_w) / (\alpha_w + \alpha_s \cdot EI_s/EI_w) \quad (1)$$

$EI_w$  is elastic bending stiffness only of glulam timber and  $EI_s$  is elastic bending stiffness  $EI_s$  of rebar based on the assumption of the plane section. On the other hand, because rebars increase bending stiffness of the composite beam, its shear force also increases in actual design, and the ratio of shear deformation to bending deformation of the beam will become larger. Thus, its shear creep also increases. Accordingly, it is necessary to estimate separately bending deformation component  $\delta_b$  and shear deformation component  $\delta_s$  in the beam's deflection  $\delta_t$ . The relative creep coefficient of shear deformation component  $\delta_s$  is designated as  $C_\gamma$ . The deflection of beam is conceptually expressed by Equation (2).

$$\delta_t = C_\phi \delta_b + C_\gamma \delta_s \quad (2)$$

## 2.3 SPECIMENS

Figure 1(a)(b) shows cross sections of specimens. The number of specimens was one for each section for the reason above. Their glulam timber, which was made of Japanese cedar, was compliant to JAS-identical grade E65-F255. Rebar was compliant to JIS-identical SD390 and its size was D29. Six of each rebars were embedded in two layers at the upper compressive and lower tensile sides within beam section. In actual beams, each additional lamina is bonded to the upper and lower surface for fire resistance as shown in Figure 1(c). When designing, the structural performance of that additional lamina will not be estimated on structural safety. Although moisture penetrates the surface of timber as mentioned in Chapter 1, the adhesive layer of the additional lamina prevents the penetration into wood around rebars in lamina which are on the upper and lower surfaces of beam. The additional laminas were designed to provide only protection from moisture absorption without reducing the deformation component of bending creep. For this reason, 30 mm thick additional laminas were bonded to the upper and lower surfaces of the beam and then were planed down to 3.5 mm thickness as shown in Fig. 1(a)(b). Resorcinol resin adhesive was used to bond the laminas. An arrangement of strain foil gauges and displacement transducers will be mentioned in Section 2.5. The length of glulam timber beam was 3706 mm, and a composite beam was 9210 mm. Figure 2 illustrates the process for embedding rebar to the lamina. Three row U-shaped grooves were grooved to a lamina and rebars were placed in each groove. Wood covers were bonded over the grooves and epoxy resin adhesive was injected into the groove after curing adhesives for one day. A heat-resistant epoxy adhesive acceptable up to 110°C was used for these adhesives. Table 1 summarizes properties of the adhesive.



Timber: Glulam, Japanese Cedar/E62F225  
Average 3.5mm laminas bonded to upper and lower surfaces

Figure 1: Cross-section of specimens

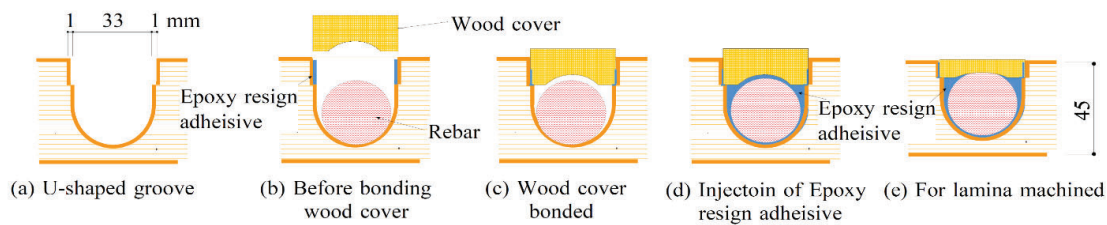


Figure 2: Process for embedding rebar into lamina (Unit: mm)

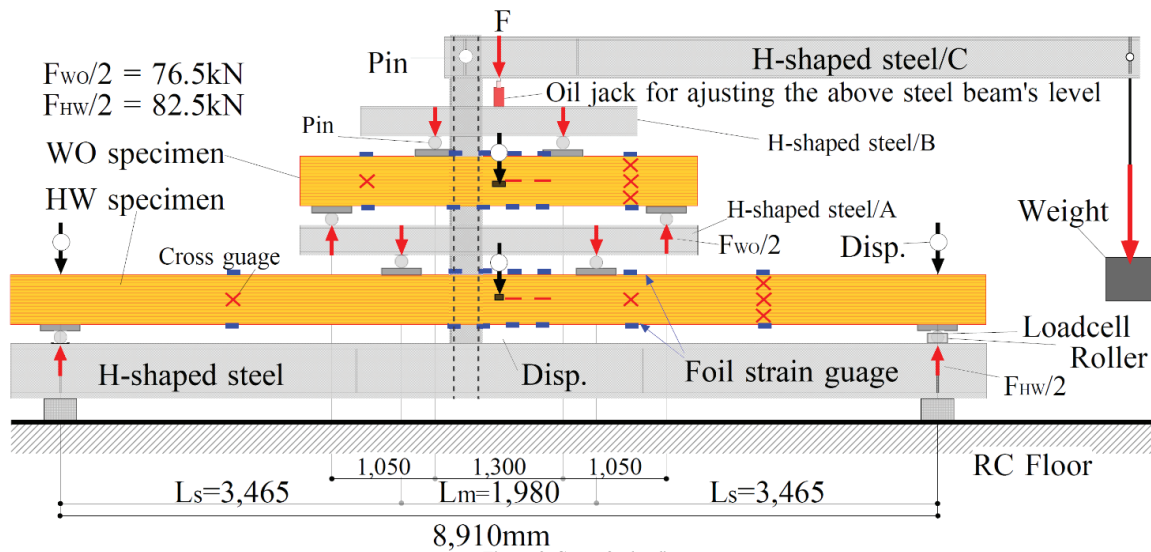


Figure 3: Setup for loading

## 2.4

Table 1: Properties of Epoxy adhesive

$E$		
2700	110	60

$E$ : Young's modulus in  $N/mm^2$

$F_c$ : Compressive strength

$c_s$ : Shearing strength by compression

## EXPERIMENTAL METHOD

Figure 3 illustrates the four-point bending arrangement setup for the loading test. A glulam timber beam was stacked on top of a hybrid timber beam and a single loading apparatus can be used to load both beams. The vertical reaction force at the fulcrum of one side of the hybrid timber beam was measured with a load cell. The load applied to the test specimen is calculated by subtracting the weight of the beam specimens and the H-shaped steel beam from the load measured by the load cell if needed. The load through the H-shaped steel C was applied to the middle of the span length of the steel and specimens. As the deflection progresses, the H-shaped steel beam C inclines to rotating shaft pin, and the load on the beam decreases, therefore the steel beam C was adjusted to the leveling using a hydraulic jack (capacity: 200 kN, stroke: 126 mm) which was located at the loading position between the steel beam C and B, and the

load measured by the load cell maintains a constant value. The vertical load on steel beam B was applied by load W was hung from the end of the steel beam C. The loading position was applied to a force approximately 33.7 times the weight of W. Photo 1 shows the loading situation. Photos 1(A) to (F) are enlarged photos of the yellow circled areas in the whole view. Load W hangs from upper steel beam as seen on the right of the whole view. As shown in Photo 1(A), steel channel pillars were bound to the wall with steel plates and bolts. This allowed for the installation of the beams and the H-shaped steel beam. The beams and H-shaped steel beams could move only vertically between the two pillars. Applying grease between a plate on the beam and a plate on the pillars as in Photo 1(B) allowed to the specimens gliding between the two pillars. The movement of the upper steel beam was restricted by the steel channel pillars. Photo 1(C) shows the load cell installed at the right support point of the HW beam. A sphere is placed between the beam and the load cell and functions as a universal joint. Photo 1(D) shows a one-way roller at the left support point of the HW beam. The specimen with the one-way roller at the left end and the universal joint at the right end was stable and didn't experience unexpected stresses. Photo 1(E) shows the oil jack. The oil jack keeps the upper steel beam in a horizontal position. The oil jack was placed on the loading point so that the force applied to the H-shaped



View of set-up for loading



A: Plates for vertical sliding to H-shaped steel/C



B: Plates for vertical sliding to specimens



C: Loadcell and universal pin



D: One-way roller



E: An oil jack for adjusting the level of H-shaped steel/C and one-way pin



F: Displacement transducer for deflection of WO

Photo 1: Setup for loading

steel beam and specimens would occur through the oil jack. The deflection in the WO beam was measured as shown in Photo 1(F). Displacement transducers were installed on steel frame placed on top at the front and rear of the WO beam. This method can measure the vertical deformation of the beam relative to both support points using only two transducers.

## 2.5 MEASUREMENT OF DEFLECTION AND STRAIN

Figure 4(a)(b)(c) show the location of measuring the deflection and the strain of the beam and these methods. In the hybrid timber beam, the vertical deformation at the middle span of front and rear of the beam and at both of support points were measured using displacement transducers. The deflection of the beam was calculated by subtracting the average vertical deformation at both support points from the average vertical deformation at the middle span of the beam. In the laminated timber beams, the vertical deformation of the middle span of the beam relative to at both support points were measured at the front and rear of the beam, as shown in Figure 4(c). The deflection of the beam is the average them. As shown in Figure 4(a)(b), axial strain of the wood was measured by strain gauges attached to the upper and lower of the beam, and shear strain was measured by strain gauges the front of the beam. Foil strain gauges (length: 60mm) for long-term measurements were used. There are four locations that measured the axial strain at the pure bending span of glulam timber and two gauges were attached per a location. In the shear span of the beam, shear strains were measured at a location on the left side and two locations on the right. In the front of the beam, the shear strain was measured by cross strain gauges attached to, and the bending strain was measured by strain gauges attached to the neutral axis between the pure bending span. Strain gauges attached to the rebar at the location of the middle span of the beam measured the axis strain of the rebar. The foil strain gauges (length: 2mm) were attached to the front and rear of the rebar per a location. The axis strain of the rebar is the average two values of the front and back gauges of the rebar. We used ordinary foil strain gauges and adhesive for attaching the rebar because the gauges were coated by the epoxy adhesives in the groove.

## 2.6 START OF THE LONG-TERM LOADING TEST

The span length of the composite beam was determined so that the maximum bending stress of the beam and the shear stress at the neutral axis were equal to their respective long-term allowable stresses. Table 2 lists calculated values of maximum bending stress  $\sigma_{wb}$ , shear stress  $\tau_w$ , axial stress of the rebar  $\sigma_r$ , and their allowable

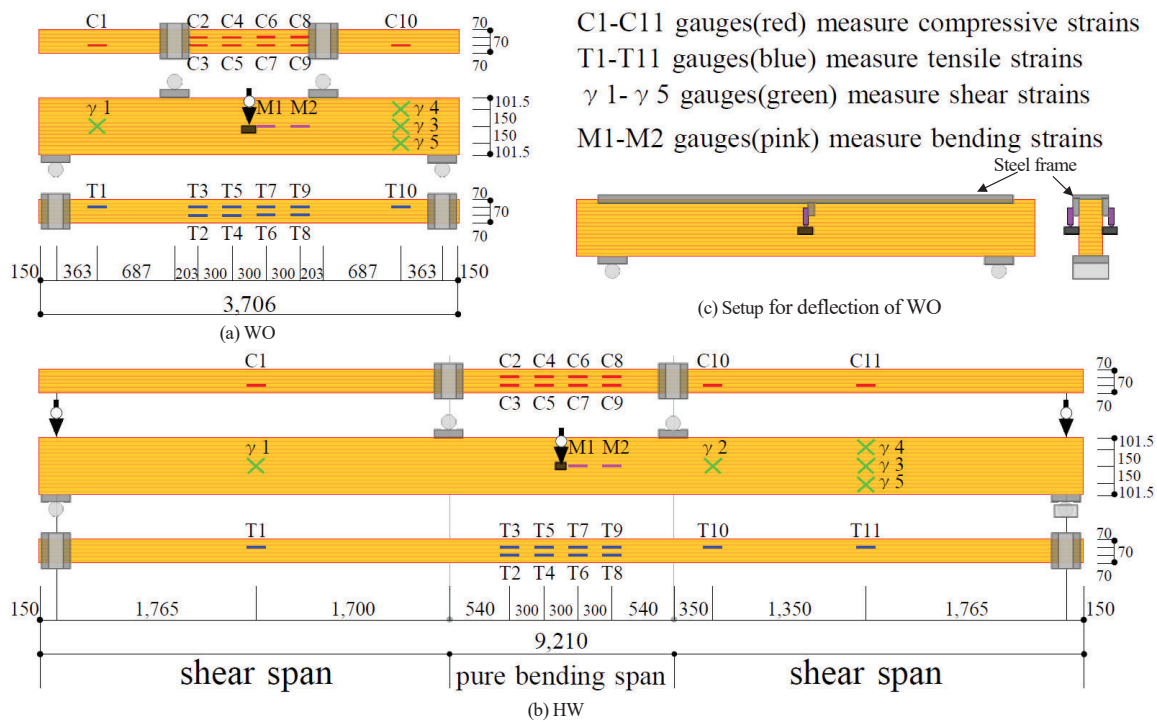


Figure 4: Views of specimens and configuration of rebar arrangement of HW

Table 2: Maximum bending stress and shear stress of wood and maximum axial stress of rebar in beam

Specimen	$Q$ kN	$M_m$ kNm	$\sigma_w$ N/mm <sup>2</sup>	$\sigma_{wa}$ N/mm <sup>2</sup>	$\sigma_w/\sigma_{wa}$	$\sigma_r$ N/mm <sup>2</sup>	$\sigma_{ra}$ N/mm <sup>2</sup>	$\sigma_r/\sigma_{ra}$	$\kappa_s$	$\tau_w$ N/mm <sup>2</sup>	$\tau_{wa}$ N/mm <sup>2</sup>	$\tau_w/\tau_{wa}$
WO	76.5	80.3	9.56	8.25	1.16	-	-	-	1.50	1.09	0.99	1.10
HW	82.5	279.9	8.35		1.01	187	195	0.96	1.34	1.05	0.99	1.06

stresses of the glulam timber when long-term loading. The long-term allowable bending stress for the glulam timber is 8.25 N/mm<sup>2</sup> for bending stress, 0.99 N/mm<sup>2</sup> for shear stress, and 195 N/mm<sup>2</sup> for axial stress for the rebar. Ignoring the beam's own weight, the vertical reaction force measured by the load cell placed at the right supports of specimen is equal to the shear force  $Q$  of the beam. The self-weight of the hybrid timber beam (HW) is 0.99 kN/m, the glulam timber beam (WO) is 0.37 kN/m, and the H-shaped steel beam A is 2.95 kN.

The shear force  $Q$  of the beam was calculated ignoring the own weight, while the bending moment  $M_m$  at the midspan of the beam was calculated using the own weight. The loading was set according to the bending stiffness to equal the bending stress and the long-term allowable stress in both beams. First, the value of load on the HW was calculated using Young's modulus of the glulam timber and rebars as the reference value. The weight at the right end of the H-shaped steel beam C was set so that the deflection at the upper and lower surface of HW reached a target value. The loading of the beam

increased in proportion to the bending stiffness of the beam so that the bending stress of the beam was equal to the long-term allowable stress. The bending Young's modulus of the glulam timber was determined based on the moment-curvature relationship of the WO obtained by this load. This load was removed once, and the load was applied again after the loading positions of two loading points on WO were corrected, based on the measured Young's modulus. Young's modulus of the rebar was set to the standard value of 2.05x10<sup>5</sup> N/mm<sup>2</sup>, and the bending Young's modulus of the glulam timber was determined to be 8,200 N/mm<sup>2</sup>, which is the average of the values calculated from 10 bending stiffnesses at 10 cross-sectional positions of the WO. These values are summarized in Table 2. Table 2 also lists the ratio of maximum stress to the allowable stress for each. Each stress in the HW beam was nearly equal to the allowable stress, while the bending stress in the WO beam exceeded the long-term allowable stress by 16 % and the shear stress by 10 %. Long-term loading was started under these conditions.

### 3 – RESULTS

#### 3.1 LOAD-DEFLECTION RELATIONSHIP DURING INTRODUCING LONG-TERM LOAD

The first loading test started on December 20, 2023, but the test was redone on December 26 to be correct the loading position of the beam.

Figures 5 through 7 show various relationships at the start of the first and second loading tests. Figure 5 shows a moment-curvature relationship. The curvature is determined from the average of two strain gauges value attached to the top and bottom of the beam. Temperature correction allowed to accurately estimate the strain of the beam. The moments at each position of the strain gauges were shown in Figure 5. The average value of Young's modulus for the glulam timber beam ( $8.20 \times 10^3 \text{ N/mm}^2$ ) was obtained from the results in Figure 5(a). The pink dash-dotted line in Figure 5(a)(b) show the bending stiffness of the Glulam timber calculated using this value. In the second loading, residual strain that occurred during the unloading of the first loading resulted in a curvature at the zero loaded point. Ignoring this residual curvature,

the calculated value of bending stiffness of the beams can approximately estimate the stiffness in the second loading. The pink dash-dotted line for HW in Figure 5(c)(d) indicates the bending stiffness of the timber composite beam calculated with the average Young's modulus of the glulam timber/WO obtained earlier and the standard value for Young's modulus of the rebar. The stiffness calculated was only about 2% larger than the average experimental stiffness and estimates the experimental stiffness with good accuracy.

Figure 6 shows the shear stress-shear strain relationship at the mid-high of beam depth. Shape factor of shear stress in the beam theory is 1.5 for WO beam and 1.34 for HW beam. The pink dash-dotted line in Figure 6(a)(b) is the average shear modulus of the beam ( $1100 \text{ N/mm}^2$ ) calculated from the shear stress-shear strain relationship of the WO in the first loading. The experimental stiffness in the first loading for HW beam was about 15% lower than the stiffness calculated using the shear modulus of WO above. The shear span length of WO is short, and hence the shear stress intensity based on the assumption of the plane section for beam may greatly overestimate the actual shear stress intensity. In subsequent calculations, the average of the respective shear modulus

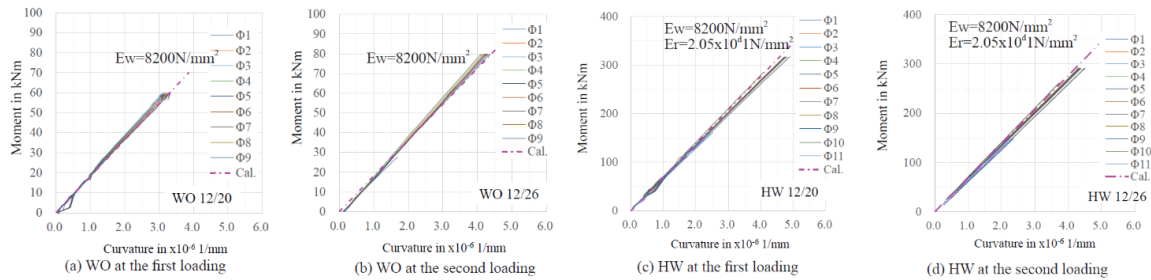


Figure 5: Moment-curvature relationship during introducing load

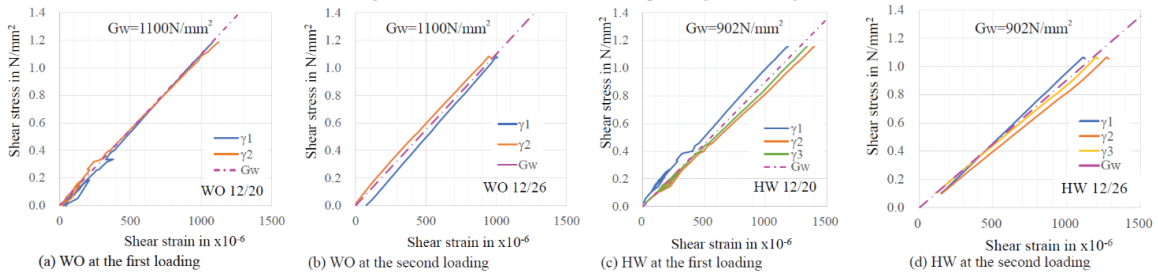


Figure 6: Shear stress-shear strain relationship of web during introducing load

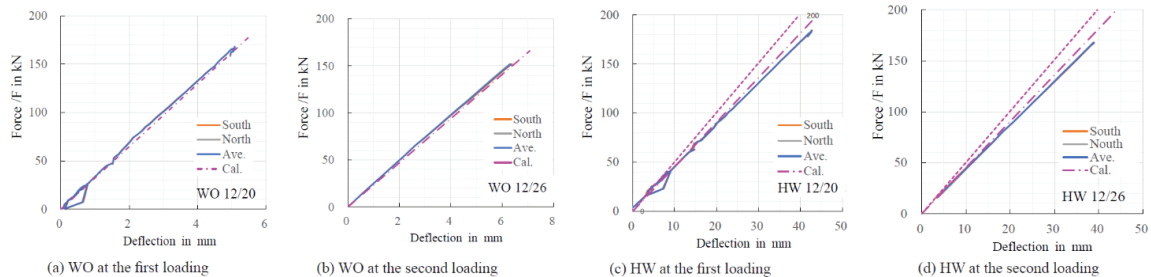


Figure 7: Force-deflection relationship during introducing load

determined from the first loading will be used for WO and HW each.

Figure 7 shows the load-deflection relationship. The pink dash-dotted line in Figure 7 was the stiffness of deflection due to the sum of the calculated bending and shear deformation components. Also, the pink dotted line in Figure 7(c)(d) was the deflection of only bending deformation in HW. There is a certain difference between the dotted line and the experimental stiffness; the difference demonstrates that shear deformation must be added for HW. For WO, the calculated stiffness estimates with good accuracy the experimental stiffness. For HW, the experimental stiffness becomes smaller than the calculated stiffness for the range of more than 100 kN.

### 3.2 CREEP DURING LONG-TERM LOADING

Figure 8 shows changes of temperature (Temp.), relative humidity around the specimens (RH), deflection ( $\delta$ ), and half of vertical load ( $F/2$ ), i.e., beam shear force, during long-term loading. As the force decreases as the specimen deflection increases, the steel beam C was periodically levelled with the oil jack shown at the top of Figure 2 so that the shear force of HW ( $F/2$ ) was maintained at 82.5 kN. The shear force of WO is less than HW because WO is placed on top of HW and the steel

beam B. Temperature began to increase significantly on March 28<sup>th</sup>, reaching about 30°C between July and September in 2024, then decreasing to about 10°C in January in 2025. Relative humidity/RH fluctuated between 40-80%. The WO deflection/ $\delta_{WO}$  is small relative to HW, due to the short span length of WO. HW's deflection/ $\delta_{HW}$  changed gradually in response to temperature fluctuations. Figure 9 shows the variation of curvature at each location in the pure bending span. The curvature of WO increased from March 28<sup>th</sup> in 2024 with increasing temperatures, while increase in the curvature of HW was very small relative to WO. The bending moment at the pure bending span is 80.3 kNm for WO and 279.8 kNm for HW. Despite the bending moment of HW being 3.5 times larger than WO, the increase in the curvature of HW was very small. The result demonstrates the rebar reduces the creep of the curvature. Figure 10(a)(b) shows variations of strain at locations of the upper and lower surfaces of beam's timber. Numbering of the strain is same as that of the curvature at the locations each. Strains on the lower side, i.e. tensile side, of WO has a small variation and varies gradually, while those on the upper side, i.e. compressive side, shows more variation and a larger increase than the tensile side. In contrast, strains of HW have little variation on the compressive and tensile sides. Figure 10(c) shows

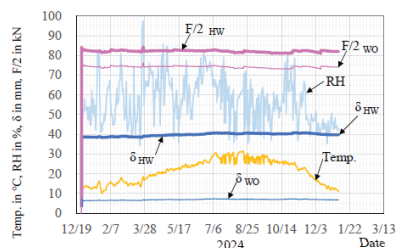


Figure 8: Changes of temperature/Temp, relative humidity/RH, deflection/ $\delta$ , and force/F

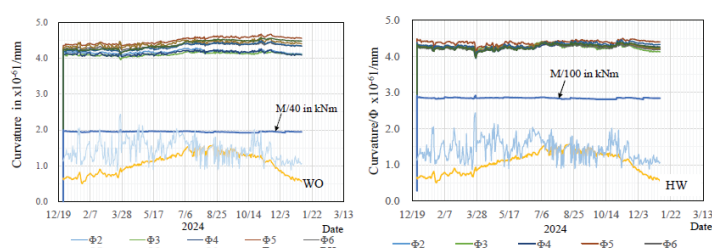
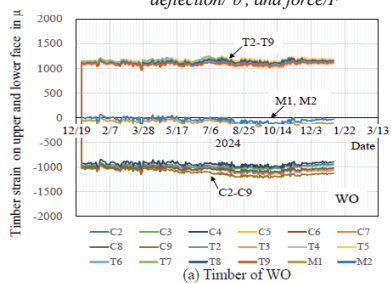
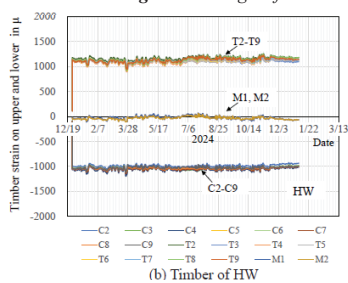


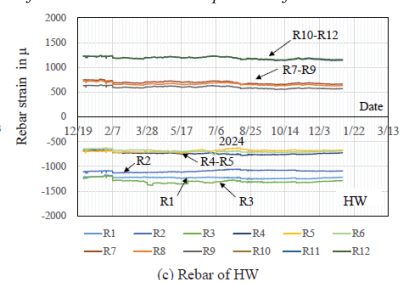
Figure 9: Changes of curvatures of timber at each measure position of timber



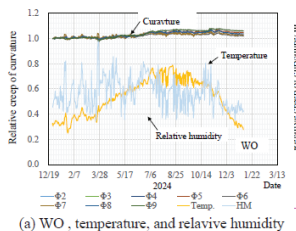
(a) Timber of WO



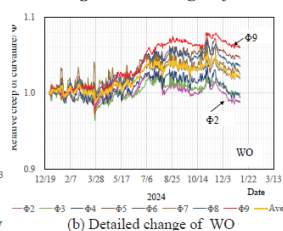
(b) Timber of HW



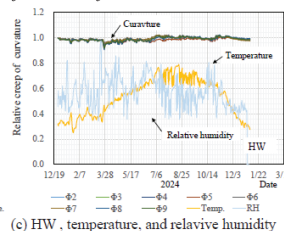
(c) Rebar of HW



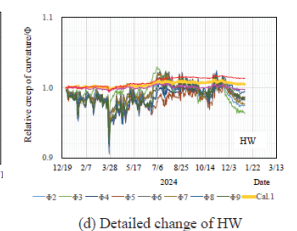
(a) WO, temperature, and relative humidity



(b) Detailed change of WO



(c) HW, temperature, and relative humidity



(d) Detailed change of HW

Figure 11: Changes of relative creep of curvature at each measure position of timber

variation in axial strain for each rebar. In the upper rebars (R1-R3), strain of R2 was smaller relative to R1 and R3 from the start of loading, while the strain of the other compressive and tensile rebars slightly increased from April-September. Figure 11 shows relative creep of curvature. Figure 11(b)(d) is an enlarged view of the vertical axis of Figure 11(a)(c). Variation owing to their locations is larger for the WO than for HW, and the relative creep is also larger for the WO. Figure 12 shows variation of shear strain. The warm color curves indicate curves by shear strain of WO; the cold colors indicate those of HW. HW has higher strain because shear force of beam is subjected to is greater than that of WO. Figure 13 shows the relative creep of shear strain of timber. The pink curve is change in average value at each location. The change in their averages was almost the same for both WO and HW, with an increase to approximately 1.3 since March 28<sup>th</sup> in 2025. Relative creep of shear strain was larger than that of curvature.

### 3.3 ESTIMATION OF CREEP COEFFICIENT

Figure 14 shows change of relative creeps of curvature, deflection, and shear strain. Curvature and shear strain are the average value at each location. Curvature and deflection increased from March 28<sup>th</sup> to July in 2024 for both WO and HW, remained constant, and after then decreased from December in 2024. In contrast, shear strain increased by a large amount from March 28<sup>th</sup> to

September in 2024 and then increased gradually. Relative creep calculated for HW's curvature is shown in Figure 14(b) as a thick yellow curve. The relative creep was calculated, using the average curve of relative creep of curvature of WO and Equation (1). The relative creep of deflection determined from the shear and bending deformation of HW and Equation (2) is shown by the thick blue curves. Shear deformation was calculated using the average curve of relative creep of shear strain of HW. Relative creep of curvature and deflection of HW beam is still small, however, and the creep of each has been almost estimated by the curve calculated. The pink, red, and yellow curves in Figure 11(d) indicate curves calculated for the relative curvature creep of HW. The curves were obtained by Equation (1) using the minimum ( $\Phi 2$ : pink), maximum ( $\Phi 9$ : red) and average (yellow) values of the curvature creep of WO in Figure 11(b). While the calculated curves did not capture the fine changes observed in the experimental curves, they did roughly capture the changes. The creep of the bending deformation component has almost been estimated by Equation (1) as the present time. We can conclude that the decrease in the shear stiffness of HW beam caused by the moisture absorption at wood around rebar mentioned Chapter 1 did not nearly occur.

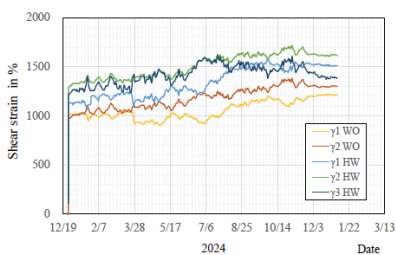


Figure 12: Changes of shear strains of timber web

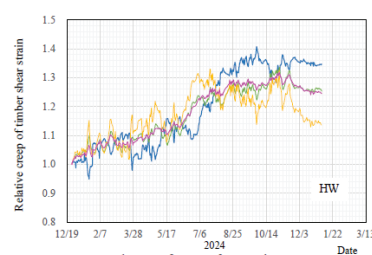


Figure 13: Changes of relative creep of shear strains of timber web

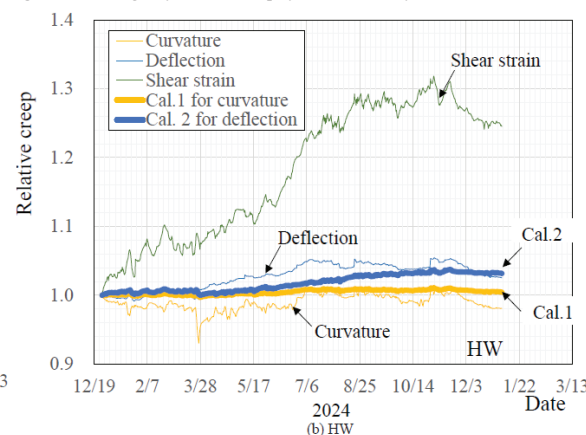
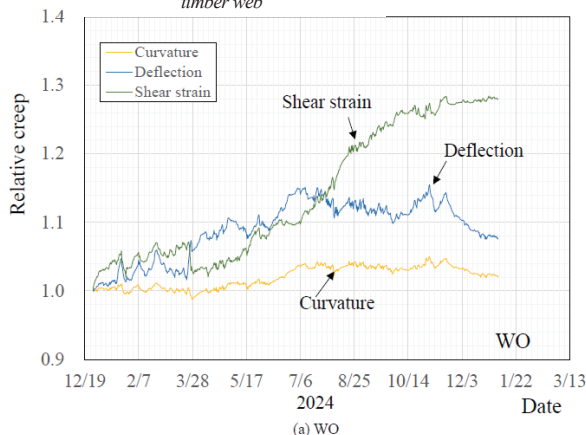


Figure 14: Changes of relative creep of curvatures of timber, deflection of beam, shear strains of timber web, and curves calculated for HW

## 4 – SUMMARY

In this study, we investigated the validity of the previous proposed estimation method with full-scale size beam specimens and the adverse effect of the moisture absorption of wood around rebar by measuring the bending deformation components at many locations in the creep experiment on one full-scale timber composite beam. The results are summarized as follows.

- i) The relative creep of the curvature and deflection of the steel bar -timber composite beam could have been estimated by Equation (1) and (2) using the measured data of the curvature creep properties of conventional Glulam timber beam with full-scale cross section and span-length.
- ii) Reduction of stress of rebar owing to decrease in shear stiffness of wood around the rebar caused by moisture penetration into timber from the surface of the beam, which occurred in the small-scale specimen, has not observed in the full-scale specimen to the present time.

## 5-ACKNOWLEDGEMENT

This project was funded as Grants-in-Aid for Scientific Research ‘A’ by Japan Society for the Promotion of Science, 2022.

## 6 – REFERENCES

- [1] S. Shioya, et al.: An innovative hybrid timber structure in Japan: performance of column and beam, Wein, WCTE 2016
- [2] N. Matsuoka, T. Izak, K. Fukudome, S. Shioya: Long-term loading test on creep of steel bar-timber composite beam, Santiago, WCTE 2021